AIAA JOURNAL
Vol. 41, No. 9, September 2003

Asymptotic Finite Elements Introducing the Method of Integral Multiple Scales

James W. Rogers Jr.*
U.S. Air Force Research Laboratory, Wright–Patterson Air Force Base, Ohio 45433
and
Gregory S. Agnes†
Air Force Institute of Technology, Wright–Patterson Air Force Base, Ohio 45433

The method of integral multiple scales (MIMS) is introduced and applied to linear and nonlinear beam models. Based on the method of multiple scales, MIMS is applied to the system Lagrangian and directly results in a system solution. An analytical solution approach is applied to a linear beam-string model to produce a system of linear differential equations that can be solved to produce an asymptotic solution. The true power of MIMS is then demonstrated through a finite element approach by using a set of parametric shape functions based on beam strings. Where the analytic methodology is limited to continuous systems, the finite element approach is easily applied to discontinuous systems providing an analysis method useful with distributed piezoelectric laminates. Both static and dynamic results are discussed. The use of the asymptotic shape functions in the MIMS asymptotic finite element method results in extremely high precision and provides a methodology that could provide a more efficient analytical tool for the development of highly compliant discontinuous systems.

Nomenclature

A	=	cross-sectional area
$[\boldsymbol{C}]_{n\times n}$	=	system damping matrix
c_1, c_2	=	axial, transverse speed of sound
d_{31}	=	piezoelectric constant
$\{\boldsymbol{d}(t)\}_{n\times 1}$	=	displacement vector
E	=	Young's modulus
EA	=	axial stiffness
EI	=	bending stiffness
g	=	independent variable (x, t)
$[\boldsymbol{K}]_{n\times n}$	=	system stiffness matrix
L	=	beam length
$\mathbb{L}$	=	Lagrangian
$[\boldsymbol{M}]_{n\times n}$	=	system mass matrix
N_i	=	initial axial load
$\{\boldsymbol{N}(x)\}_{1\times n}$	=	shape function vector
P	=	pressure differential
q	=	order
r	=	radius of gyration
T	=	timescales
$\mathbb{T}$	=	kinetic energy
t	=	time
t^*	=	thickness
u, w	=	displacements
$\mathcal{V}$	=	integration volume
$\mathbb{V}$	=	potential energy
$\mathbb{W}_{\text{nc}}$	=	virtual work due to nonconservative forces
w^c	=	composite asymptotic solution
x, z	=	reference axes
$\alpha, \beta, \gamma, \delta$	=	shape function boundary values
α^*, β^*	=	Rayleigh coefficients
$\bar{\alpha}$	=	thermal constant
ε	=	expansion parameter
ϵ	=	strain
ϵ_0	=	prestrain
η, ξ, ζ	=	spatial scales
$\boldsymbol{\nu}_i, \lambda_i$	=	eigenvector/eigenvalue pair
ρ	=	beam material density
σ	=	stress
σ_0	=	prestress
τ	=	scaled time
ω	=	frequency expansion

Subscripts

$, g$	=	derivative with respect to variable g
q	=	order notation

Superscripts

T	=	transpose
$\hat{}$	=	dimensional value

Introduction

EXTREMELY flexible structures present unique analysis challenges. Loads on inflatable structures, for example, produce localized effects such as buckling. Additionally, to analyze an inflatable structure of reasonable complexity, approximation methods must be employed. However, methods using standard finite element procedures require extremely dense grids to model these localized effects.

Current approximation methods coupled with computational limitations prove incapable of accurately modeling the behavior of extremely compliant high-precision structures, such as an inflatable optical space reflector, due to fundamental assumptions. In a standard finite element procedure, the underlying assumption is that the representative shape functions adequately represent the behavior of the structure being modeled. As the grid density of an inflatable structure is reduced, the portion of the model being represented by the chosen shape functions tend to behave less like the standard plate element and more as a membrane. This paper presents a new analysis method that better models such compliant systems and allows for more efficient approximation.

Received 10 May 2002; revision received 16 October 2002; accepted for publication 5 January 2003.

*Aeronautical Engineer, Air Vehicles Directorate; james.rogers2@wpafb.af.mil. Member AIAA.

†Assistant Professor, Aeronautical and Astronautical Engineering Department; gregory.agnes@afit.edu. Senior Member AIAA.

The method of integral multiple scales (MIMS) is a variation of standard multiple scales. The perturbation method of multiple scales can produce solutions to certain classes of differential equations. This paper introduces the new MIMS method and adapts it to a new finite element approach. This finite element method is applied to the linear beam string, for which the closed-form solution is well known, and comparisons are made. Then when the application is extended, a nonlinear beam-string model representing a laminate of compliant structural material and piezopolymer actuators is analyzed to further illustrate the power of this method.

This paper is the third in a four-part series presenting the development of a new methodology for the analysis of large-scale inflatable optical reflectors. The first paper developed the mechanics of extremely compliant one-dimensional beams with very small thickness to length ratios termed beam-strings.[1] The second paper expanded this methodology to represent the two-dimensional plate of extreme compliance and very small thickness to area rations termed plate-membranes.[2] The fourth will present the application of the MIMS method to a discontinuous axisymmetric active membrane.[3]

Linear Beam String

Nayfeh presents the linear beam-string problem using both the method of matched asymptotic expansions[4] and the method of multiple scales when a system has a single boundary layer.[5] Herein, the method of multiple scales is expanded to include multiple boundary layers. To develop the necessary fundamental equations needed in this analysis, the system Lagrangian is needed. The potential energy of a clamped–clamped elastic beam, assuming plane sections remain plane, can be defined using the strain energy representation:

$$\hat{\mathbb{V}} = \frac{1}{2}\int_{\hat{\mathcal{V}}} E\hat{w}_{,\hat{x}}^2 - 2E\hat{z}\hat{w}_{,\hat{x}}\hat{w}_{,\hat{x}\hat{x}} + E\hat{z}^2\hat{w}_{,\hat{x}\hat{x}}^2 \,\mathrm{d}\hat{\mathcal{V}} \tag{1}$$

The beam's kinetic energy, ignoring rotatory inertia, can be represented as

$$\hat{\mathbb{T}} = \frac{1}{2}\int_{\hat{\mathcal{V}}} \rho\hat{w}_{,\hat{t}}^2 \,\mathrm{d}\hat{\mathcal{V}} \tag{2}$$

The system's virtual work due to a pressure force and can be represented as

$$\hat{\mathbb{W}}_{\mathrm{nc}} = -\int_{\hat{x}} \hat{P}\hat{w}\,\mathrm{d}\hat{x} \tag{3}$$

The simple beam's Lagrangian can then be formed using Eqs. (1–3), and the equations of motion can be derived using

$$\int_{\hat{t}_1}^{\hat{t}_2} \delta\hat{\mathbb{T}} - \delta\hat{\mathbb{V}} + \delta\hat{\mathbb{W}}_{\mathrm{nc}}\,\mathrm{d}\hat{t} = 0 \tag{4}$$

and Hamilton's principle, where δ indicates variation in this equation. This system's dimensional Lagrangian is then

$$\hat{\mathbb{L}} = \frac{1}{2}\int_{\hat{\mathcal{V}}} \rho\hat{w}_{,\hat{t}}^2 - E\hat{w}_{,\hat{x}}^2 - E\hat{z}\hat{w}_{,\hat{x}\hat{x}}^2 \,\mathrm{d}\hat{\mathcal{V}} - \int_{\hat{x}} \hat{P}\hat{w}\,\mathrm{d}\hat{x} \tag{5}$$

with clamped boundary conditions.

The equation of motion for this system can be quickly verified as

$$\rho A\hat{w}_{,\hat{t}\hat{t}} + EI\hat{w}_{,\hat{x}\hat{x}\hat{x}\hat{x}} - EA\hat{w}_{,\hat{x}\hat{x}} = -\hat{P} \tag{6}$$

which is the dynamic linear Bernoulli–Euler beam equation. Applying the scaling relations $w = \hat{w}/L$, $z = \hat{z}/L$, $x = \hat{x}/L$, and $\mathrm{d}x = \mathrm{d}\hat{x}/L$ and letting

$$\varepsilon^2 = EI/EAL^2, \qquad P = \hat{P}L/EA, \qquad t = \sqrt{(\rho AL^2/EA)}\,\hat{t} \tag{7}$$

in Eq. (5) produces

$$\mathbb{L} = \int_x \left[\frac{1}{2}w_{,t}^2 - \frac{1}{2}w_{,x}^2 - \frac{1}{2}\varepsilon^2 w_{,xx}^2 - Pw\right]\mathrm{d}x \tag{8}$$

where ε is the scaled radius of gyration of the beam and represents the "smallness" parameter that lends this system to perturbation solution methods.

With the energy representation of a system available, various methods are available to compute an analytic solution for simplified problems or to determine an approximate solution for more complex problems. The MIMS provides one such solution methodology. With roots in standard perturbation methods, MIMS produces a system of equations to be solved in succession to produce an asymptotic solution.

Analytical Solution

To validate the asymptotic finite element solutions, an analytical solution is required for test case(s). When dynamic effects are ignored a standard matched asymptotic expansion of on Eq. (6) produces a system of differential equations whose solutions are blended together to produce an adequate approximation. The outer expansion, which dominates in the central portion of the beam, is represented in general by the following differential equation:

$$w_{i,xx} = f(x, w_j, w_{j,x}) \tag{9}$$

where $j < i$ and $i, j \geq 0$. The subscripts j, i represent the perturbation expansion order for a given equation. The solution to the homogeneous equation is a quadratic polynomial. The inner expansions, which dominate the boundary area at either end of the beam, are represented in general by the following differential equation:

$$w_{i,\xi\xi\xi\xi} - w_{i,\xi\xi} = f(\xi, w_j, w_{j,\xi}, w_{j,\xi\xi}, w_{j,\xi\xi\xi}) \tag{10}$$

$$w_{i,\zeta\zeta\zeta\zeta} - w_{i,\zeta\zeta} = f(\zeta, w_j, w_{j,\zeta}, w_{j,\zeta\zeta}, w_{j,\zeta\zeta\zeta}) \tag{11}$$

where $j < i$, $i, j \geq 0$, and

$$\xi = x/\varepsilon, \qquad \zeta = (1-x)/\varepsilon \tag{12}$$

The solutions to these equations result in additional exponentially decaying terms. The matching process merges these results to produce the following static composite solution[4]:

$$w^c = (P/2)(x - x^2) - \varepsilon[(P/2)(1 - e^{-\xi} - e^{-\zeta})] \tag{13}$$

Figure 1 shows the beam-string deflection and the effect of the smallness factor on the solution. The region where the beamlike behavior occurs is near the ends, in the boundary layers. The length of this area is roughly $\mathcal{O}(\sqrt{\varepsilon})$, which is directly related to the beam's thickness-to-lengthratio. The dramatic impact of ε on the solution is apparent. Note that the region of validity is finite. An initial assumption was that ε was very small. If ε is too large, the solution breaks down as the boundary regions begin to significantly encroach on each other. This is representative of a common limitation in all perturbation methods.

Integral Multiple Scales

Equation (8) produces a beam-string solution, which near its ends exhibits beamlike behavior and in the center region acts like a membrane. This suggests a spatial multiple scales application. Multiple scales is commonly applied to the differential equations of motion resulting from application of variational principles. The approach presented here is the MIMS, which is applied directly to the system Lagrangian. The result is an integrated solution, bypassing the cumbersome matching process.

Based on a priori knowledge of the system (the analytical solution in the preceding section) we can safely assume the distinguished parameter is 1 in this application. Three scales [$\eta = x$, $\xi = x/\varepsilon$, and $\zeta = (1-x)/\varepsilon$] are applied to the Lagrangian in Eq. (8). The primary

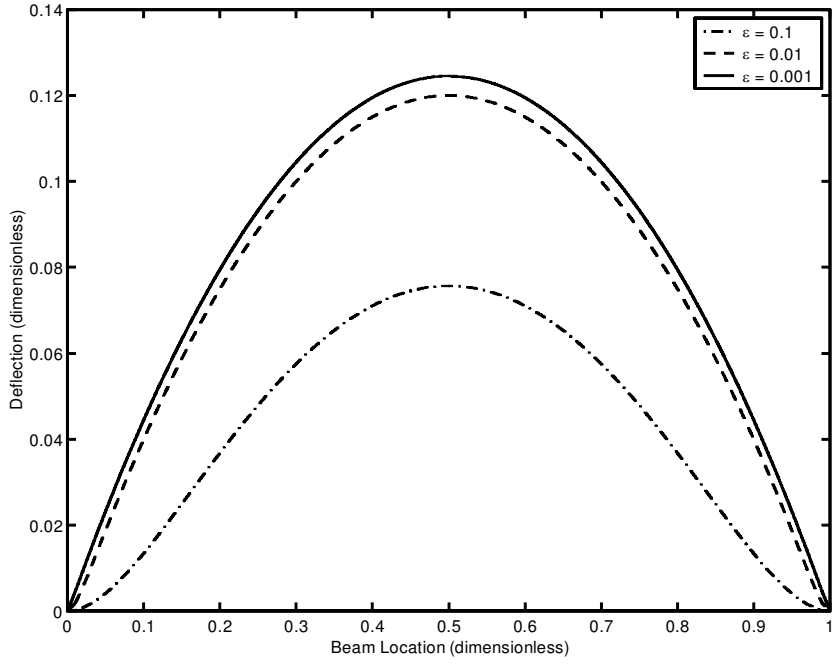

Fig. 1 Beam-string solution, $P = 1$.

assumption with the multiple scales method is that these scales are independent. The method introduced here relies on this assumption.

When the chain rule is applied to $x = x(\eta, \xi, \zeta; \varepsilon)$, the following differentials are produced:

$$\frac{\mathrm{d}}{\mathrm{d}x} = \frac{\partial}{\partial \eta} + \frac{1}{\varepsilon}\left[\frac{\partial}{\partial \xi} - \frac{\partial}{\partial \zeta}\right] \tag{14}$$

$$\frac{\mathrm{d}^2}{\mathrm{d}x^2} = \frac{\partial^2}{\partial \eta^2} + \frac{2}{\varepsilon}\left[\frac{\partial^2}{\partial \xi\,\partial \eta} - \frac{\partial^2}{\partial \zeta\,\partial \eta}\right] + \frac{1}{\varepsilon^2}\left[\frac{\partial^2}{\partial \xi^2} + \frac{\partial^2}{\partial \zeta^2} - 2\frac{\partial^2}{\partial \xi\,\partial \zeta}\right] \tag{15}$$

Substituting Eqs. (14) and (15) into Eq. (8) produces the multiple scales representation of the beam-string's Lagrangian:

$$\mathbb{L} = \int_x \frac{1}{2}w_{,t}^2 - \frac{1}{2}\left[w_{,\eta} + \frac{1}{\varepsilon}(w_{,\xi} - w_{,\zeta})\right]^2 - Pw$$

$$- \varepsilon^2\frac{1}{2}\left[w_{,\eta\eta} + \frac{2}{\varepsilon}(w_{,\xi\eta} - w_{,\zeta\eta}) + \frac{1}{\varepsilon^2}(w_{,\xi\xi} + w_{,\zeta\zeta} - 2w_{,\xi\zeta})\right]^2 \mathrm{d}x \tag{16}$$

where $w(x, t) = w(\eta, \xi, \zeta, t; \varepsilon)$. Next, substituting the expansions (note temporal scales introduced)

$$T_n = \varepsilon^n \tau \tag{17}$$

$$t = \omega\tau \tag{18}$$

$$\omega = \omega_0 + \varepsilon\omega_1 + \varepsilon^2\omega_2 + \cdots \tag{19}$$

$$w(\eta, \xi, \zeta, t; \varepsilon) = w_0(\eta, \xi, \zeta, t) + \varepsilon w_1(\eta, \xi, \zeta, t) + \cdots \tag{20}$$

where $\omega_0 = 1$ as the original system was effectively scaled by $\hat{\omega}_0$, into Eq. (16). The Lagrangian can now be organized into increasing orders of ε:

$$\mathbb{L} = \varepsilon^{-2}\mathbb{L}_{-2} + \varepsilon^{-1}\mathbb{L}_{-1} + \mathbb{L}_0 + \varepsilon\mathbb{L}_1 + \varepsilon^2\mathbb{L}_2 + \cdots \tag{21}$$

where

$$\mathbb{L}_{-2} = \int_x \frac{1}{2}F_0^2 + \frac{1}{2}G_0^2\,\mathrm{d}x \tag{22}$$

$$\mathbb{L}_{-1} = \int_x F_0F_1 + G_0G_1\,\mathrm{d}x \tag{23}$$

$$\mathbb{L}_0 = \int_x \frac{1}{2}F_1^2 + F_0F_2 + \frac{1}{2}G_1^2 + G_0G_2 - Pw_0 + \frac{1}{2}w_{0,0}^2\,\mathrm{d}x \tag{24}$$

$$\vdots$$

$$F_i = w_{i,\xi\xi} + w_{i,\zeta\zeta} - w_{i,\xi\zeta} + 2(w_{i-1,\xi\eta} - w_{i-1,\zeta\eta}) + w_{i-2,\eta\eta}$$

$$G_i = w_{i,\xi} - w_{i,\zeta} + w_{i-1,\eta} \tag{25}$$

Applying standard variational principles to each $\mathbb{L}_i$ produces

$$\mathbb{L}_{-2} : \nabla^2\left[\nabla^2 w_0 - w_0\right] = 0 \tag{26}$$

$$\mathbb{L}_{-1} : \nabla^2\left[\nabla^2 w_0 - w_0\right] = 0$$

$$\nabla^2\left[\nabla^2 w_1 - w_1\right] = -\nabla\left[4\nabla^2 w_0 - 2w_0\right]_{,\eta} \tag{27}$$

$$\mathbb{L}_0 : \nabla^2\left[\nabla^2 w_0 - w_0\right] = 0$$

$$\nabla^2\left[\nabla^2 w_1 - w_1\right] = -\nabla\left[4\nabla^2 w_0 - 2w_0\right]_{,\eta}$$

$$\nabla^2\left[\nabla^2 w_2 - w_2\right] = -\nabla\left[4\nabla^2 w_1 - 2w_1\right]_{,\eta}$$

$$-\left[6\nabla^2 w_0 - w_0\right]_{,\eta\eta} - w_{0,00} - P \tag{28}$$

where

$$\nabla = \frac{\partial}{\partial \xi} - \frac{\partial}{\partial \zeta}, \qquad \nabla^2 = \frac{\partial^2}{\partial \xi^2} + \frac{\partial^2}{\partial \zeta^2} - 2\frac{\partial^2}{\partial \xi\,\partial \zeta} \tag{29}$$

Notice that all lower solutions exist within each successive level. This allows selection of the desired level of precision at the beginning of the solution method. Therefore, if the desired solution is to be to $\mathcal{O}(\varepsilon^2)$, select $\mathbb{L}_2$ and apply the desired variational principles. When Euler's equations are applied to $\mathbb{L}_2$, the following system of equations is produced:

$$\nabla^2\left[\nabla^2 w_0 - w_0\right] = 0 \tag{30}$$

$$\nabla^2\left[\nabla^2 w_1 - w_1\right] = -\nabla\left[4\nabla^2 w_0 - 2w_0\right]_{,\eta} \tag{31}$$

$$\nabla^2\left[\nabla^2 w_2 - w_2\right] = -\nabla\left[4\nabla^2 w_1 - 2w_1\right]_{,\eta} - \left[6\nabla^2 w_0 - w_0\right]_{,\eta\eta} - w_{0,00} - P \tag{32}$$

$$\nabla^2\left[\nabla^2 w_3 - w_3\right] = -\nabla\left[4\nabla^2 w_2 - 2w_2\right]_{,\eta} - \left[6\nabla^2 w_1 - w_1\right]_{,\eta\eta} - w_{1,00} - [4\nabla w_0]_{,\eta\eta\eta} - 2w_{0,01} - 2\omega_1 w_{0,00} \tag{33}$$

$$\nabla^2\left[\nabla^2 w_4 - w_4\right] = -\nabla\left[4\nabla^2 w_3 - 2w_3\right]_{,\eta} - \left[6\nabla^2 w_2 - w_2\right]_{,\eta\eta} - w_{2,00} - [4\nabla w_1]_{,\eta\eta\eta} - 2w_{1,01} - 2\omega_1 w_{1,00} - w_{0,\eta\eta\eta\eta} - w_{0,11} - 2w_{0,02} - \left(2\omega_2 + \omega_1^2\right) w_{0,00} \tag{34}$$

The system can be solved in succession from Eq. (30) to Eq. (34). When all time-based derivatives are removed, a static solution can be attained. The static solution of Eq. (30) is

$$w_0(\eta, \xi, \zeta) = a_0(\eta) + a_1(\eta)e^{-\xi} + a_2(\eta)e^{-\zeta} \tag{35}$$

where the positive exponential and linear terms have already been removed in as much as, because as $\varepsilon \to 0$, the solution must be finite. Applying this result to the next equation produces

$$\nabla^2\left[\nabla^2 w_1 - w_1\right] = -\nabla\left[4\nabla^2 w_0 - 2w_0\right]_{,\eta} = 2\left[a_{1,\eta}e^{-\xi} + a_{2,\eta}e^{-\zeta}\right] \tag{36}$$

The right-hand side of this equation must lie in the null space of the adjoint of the left-hand side. This requires that the right-hand side be zero to eliminate possible secular terms. This results in a_1 and a_2 to be independent of η, which means they must be constant values. With the clamped boundary conditions, these terms are eliminated, leaving only the $a_0(\eta)$ term. Therefore, no boundary layer exists at this level. This term can be completed at the next level. The solution of Eq. (31) is then

$$w_1(\eta, \xi, \zeta) = b_0(\eta) + b_1(\eta)e^{-\xi} + b_2(\eta)e^{-\zeta} \tag{37}$$

Successive levels are solved to produce the level of precision desired. The entire solution is not continued here, but it is simple to verify the original solution produced through the matched-asymptotic expansion method [Eq. (13)] satisfies this system. Although even this trivial example proves to be challenging to solve analytically, the methodical approach can take advantage of computational techniques and be applied to a finite element method.

Finite Element Application

When the expansions

$$\omega = \omega_0 + \varepsilon\omega_1 + \varepsilon^2\omega_2 + \cdots \tag{38}$$

$$w(\eta, \xi, \zeta, t; \varepsilon) = w_0(\eta, \xi, \zeta, t) + \varepsilon w_1(\eta, \xi, \zeta, t) + \cdots \tag{39}$$

are substituted into Eq. (16), and when

$$\{\boldsymbol{N}\} = \{\boldsymbol{N}_0\} + \varepsilon\{\boldsymbol{N}_1\} + \varepsilon^2\{\boldsymbol{N}_2\} + \varepsilon^3\{\boldsymbol{N}_3\} + \cdots$$

$$\{\boldsymbol{d}\} = \{\boldsymbol{d}_0\} + \varepsilon\{\boldsymbol{d}_1\} + \varepsilon^2\{\boldsymbol{d}_2\} + \varepsilon^3\{\boldsymbol{d}_3\} + \cdots \tag{40}$$

and then orders of ε are separated, the Lagrangian can be written in as a series in ε:

$$\mathbb{L} = \varepsilon^{-2}\mathbb{L}_{-2} + \varepsilon^{-1}\mathbb{L}_{-1} + \mathbb{L}_0 + \varepsilon\mathbb{L}_1 + \varepsilon^2\mathbb{L}_2 + \cdots \tag{41}$$

Selecting the order of precision is equivalent to selecting the order of the Lagrangian. All vector brackets { } and matrix brackets [ ] will no longer be carried because the reader can discriminate between scalars, vectors, and matrices. Applying standard variational principles to the individual $\mathbb{L}_i$ terms produces

$$\mathbb{L}_{-2}: \boldsymbol{K}_{-2}\boldsymbol{d}_0 = 0 \tag{42}$$

$$\mathbb{L}_{-1}: \boldsymbol{K}_{-2}\boldsymbol{d}_0 = 0$$

$$\boldsymbol{K}_{-2}\boldsymbol{d}_1 = -\boldsymbol{K}_{-1}\boldsymbol{d}_0 \tag{43}$$

$$\mathbb{L}_0: \boldsymbol{K}_{-2}\boldsymbol{d}_0 = 0$$

$$\boldsymbol{K}_{-2}\boldsymbol{d}_1 = -\boldsymbol{K}_{-1}\boldsymbol{d}_0$$

$$\boldsymbol{K}_{-2}\boldsymbol{d}_2 = -\boldsymbol{K}_{-1}\boldsymbol{d}_1 - \boldsymbol{\Gamma}_0 - \boldsymbol{M}_0\ddot{\boldsymbol{w}}_0 - \boldsymbol{K}_0\boldsymbol{d}_0 \tag{44}$$

$$\vdots$$

where

$$\boldsymbol{K}_{-2} = \int_x \boldsymbol{G}_0^T\boldsymbol{G}_0 + \boldsymbol{F}_0^T\boldsymbol{F}_0\,\mathrm{d}x \tag{45}$$

$$\boldsymbol{K}_{-1} = \int_x \boldsymbol{G}_0^T\boldsymbol{G}_1 + \boldsymbol{G}_1^T\boldsymbol{G}_0 + \boldsymbol{F}_0^T\boldsymbol{F}_1 + \boldsymbol{F}_1^T\boldsymbol{F}_0\,\mathrm{d}x \tag{46}$$

$$\boldsymbol{K}_0 = \int_x \boldsymbol{G}_1^T\boldsymbol{G}_1 + \boldsymbol{G}_0^T\boldsymbol{G}_2 + \boldsymbol{G}_2^T\boldsymbol{G}_0 + \boldsymbol{F}_1^T\boldsymbol{F}_1 + \boldsymbol{F}_0^T\boldsymbol{F}_2 + \boldsymbol{F}_2^T\boldsymbol{F}_0\,\mathrm{d}x \tag{47}$$

$$\boldsymbol{\Gamma}_0 = \int_x \boldsymbol{F}_1^T\,\mathrm{d}x \tag{48}$$

$$\boldsymbol{M}_0 = \int_x \boldsymbol{N}_0^T\boldsymbol{N}_0\,\mathrm{d}x \tag{49}$$

$$\boldsymbol{F}_i = [\boldsymbol{N}_{i,\xi\xi} + \boldsymbol{N}_{i,\zeta\zeta} - \boldsymbol{N}_{i,\xi\zeta} + 2(\boldsymbol{N}_{i-1,\xi\eta} - \boldsymbol{N}_{i-1,\zeta\eta}) + \boldsymbol{N}_{i-2,\eta\eta}]$$

$$\boldsymbol{G}_i = [\boldsymbol{N}_{i,\xi} - \boldsymbol{N}_{i,\zeta} + \boldsymbol{N}_{i-1,\eta}] \tag{50}$$

The fundamental assumption to the method of multiple scales is the independence of the scales, that is, η, ξ, and ζ. From an energy perspective, this implies that the energy in the region of dominance for each variable dominates the energy integral. Effectively, this means we can transform the integral bounds as

$$I = \int_x f(x)\,\mathrm{d}x = \int_\zeta \left\{ \int_\xi \left[\int_\eta f(\eta, \xi, \zeta; \varepsilon)\,\mathrm{d}\eta \right] \varepsilon\,\mathrm{d}\xi \right\} \varepsilon\,\mathrm{d}\zeta \tag{51}$$

The validity of this statement can be evaluated best through the results when applied to the example beam.

Again, all lower-order equations exist in each Lagrangian element. This means the functions produced through the application of Euler's equations to $\mathbb{L}_n$ exists in the set of functions produced through the application of Euler's equations to $\mathbb{L}_m$, where $m > n$.

To produce a solution through $\mathcal{O}(\varepsilon^2)$, Euler's equations are applied to $\mathbb{L}_2$ producing the following system of equations:

$$\boldsymbol{K}_{-2}\boldsymbol{d}_0 = 0 \tag{52}$$

$$\boldsymbol{K}_{-2}\boldsymbol{d}_1 = -\boldsymbol{K}_{-1}\boldsymbol{d}_0 \tag{53}$$

$$\boldsymbol{K}_{-2}\boldsymbol{d}_2 = -\boldsymbol{K}_{-1}\boldsymbol{d}_1 - \boldsymbol{\Gamma}_0 - \boldsymbol{M}_0\ddot{\boldsymbol{d}}_0 - \boldsymbol{K}_0\boldsymbol{d}_0 \tag{54}$$

$$\boldsymbol{K}_{-2}\boldsymbol{d}_3 = -\boldsymbol{K}_{-1}\boldsymbol{d}_2 - \boldsymbol{\Gamma}_1 - \boldsymbol{M}_0\ddot{\boldsymbol{d}}_1 - \boldsymbol{K}_0\boldsymbol{d}_1 - (2\omega_1\boldsymbol{M}_0 + \boldsymbol{M}_1)\ddot{\boldsymbol{d}}_0 - \boldsymbol{K}_1\boldsymbol{d}_0 \tag{55}$$

$$\boldsymbol{K}_{-2}\boldsymbol{d}_4 = -\boldsymbol{K}_{-1}\boldsymbol{d}_3 - \boldsymbol{\Gamma}_2 - \boldsymbol{M}_0\ddot{\boldsymbol{d}}_2 - \boldsymbol{K}_0\boldsymbol{d}_2 - (2\omega_1\boldsymbol{M}_0 + \boldsymbol{M}_1)\ddot{\boldsymbol{d}}_1 - \boldsymbol{K}_1\boldsymbol{d}_1 - \left[\left(2\omega_2 + \omega_1^2\right)\boldsymbol{M}_0 + 2\omega_1\boldsymbol{M}_1 + \boldsymbol{M}_2\right]\ddot{\boldsymbol{d}}_0 - \boldsymbol{K}_2\boldsymbol{d}_0 \tag{56}$$

where

$$\boldsymbol{K}_{-2} = \int_x \boldsymbol{G}_0^T\boldsymbol{G}_0 + \boldsymbol{F}_0^T\boldsymbol{F}_0\,\mathrm{d}x \tag{57}$$

$$\boldsymbol{K}_{-1} = \int_x \boldsymbol{G}_0^T\boldsymbol{G}_1 + \boldsymbol{G}_1^T\boldsymbol{G}_0 + \boldsymbol{F}_0^T\boldsymbol{F}_1 + \boldsymbol{F}_1^T\boldsymbol{F}_0\,\mathrm{d}x \tag{58}$$

$$\boldsymbol{K}_0 = \int_x \boldsymbol{G}_1^T\boldsymbol{G}_1 + \boldsymbol{G}_0^T\boldsymbol{G}_2 + \boldsymbol{G}_2^T\boldsymbol{G}_0 + \boldsymbol{F}_1^T\boldsymbol{F}_1 + \boldsymbol{F}_0^T\boldsymbol{F}_2 + \boldsymbol{F}_2^T\boldsymbol{F}_0\,\mathrm{d}x \tag{59}$$

$$\boldsymbol{K}_1 = \int_x \boldsymbol{G}_0^T\boldsymbol{G}_3 + \boldsymbol{G}_3^T\boldsymbol{G}_0 + \boldsymbol{G}_2^T\boldsymbol{G}_1 + \boldsymbol{G}_1^T\boldsymbol{G}_2 + \boldsymbol{F}_0^T\boldsymbol{F}_3 + \boldsymbol{F}_3^T\boldsymbol{F}_0 + \boldsymbol{F}_2^T\boldsymbol{F}_1 + \boldsymbol{F}_1^T\boldsymbol{F}_2\,\mathrm{d}x \tag{60}$$

$$\boldsymbol{K}_2 = \int_x \boldsymbol{G}_2^T\boldsymbol{G}_2 + \boldsymbol{G}_1^T\boldsymbol{G}_3 + \boldsymbol{G}_3^T\boldsymbol{G}_1 + \boldsymbol{G}_0^T\boldsymbol{G}_4 + \boldsymbol{G}_4^T\boldsymbol{G}_0 + \boldsymbol{F}_2^T\boldsymbol{F}_2 + \boldsymbol{F}_1^T\boldsymbol{F}_3 + \boldsymbol{F}_3^T\boldsymbol{F}_1 + \boldsymbol{F}_0^T\boldsymbol{F}_4 + \boldsymbol{F}_4^T\boldsymbol{F}_0\,\mathrm{d}x \tag{61}$$

$$\boldsymbol{\Gamma}_0 = \int_x P\boldsymbol{N}_0^T\,\mathrm{d}x \tag{62}$$

$$\boldsymbol{\Gamma}_1 = \int_x P\boldsymbol{N}_1^T\,\mathrm{d}x \tag{63}$$

$$\boldsymbol{\Gamma}_2 = \int_x P\boldsymbol{N}_2^T\,\mathrm{d}x \tag{64}$$

$$\boldsymbol{M}_0 = \int_x \boldsymbol{N}_0^T\boldsymbol{N}_0\,\mathrm{d}x \tag{65}$$

$$\boldsymbol{M}_1 = \int_x \boldsymbol{N}_0^T\boldsymbol{N}_1 + \boldsymbol{N}_1^T\boldsymbol{N}_0\,\mathrm{d}x \tag{66}$$

$$\boldsymbol{M}_2 = \int_x \boldsymbol{N}_1^T\boldsymbol{N}_1 + \boldsymbol{N}_0^T\boldsymbol{N}_2 + \boldsymbol{N}_2^T\boldsymbol{N}_0\,\mathrm{d}x \tag{67}$$

and $\boldsymbol{F}_i$ and $\boldsymbol{G}_i$ are defined in Eq. (50).

Equations (57) and (58) represent the first solvability equations in the analysis. Because $\boldsymbol{d}_0$ is arbitrary, the system matrix $\boldsymbol{K}_{-2}$ must be trivial. Because $\boldsymbol{K}_{-2}$ represents the sum of the outer products of $\boldsymbol{G}_0$ and $\boldsymbol{F}_0$, then $\boldsymbol{N}_0$ must be only a function of η. Similarly, $\boldsymbol{K}_{-1}$ is also required to be trivial for solvability. The shape functions presented in the Appendix satisfy these conditions. When these solvability conditions are imposed, the following system of equations remains [to $\mathcal{O}(\varepsilon^2)$]:

$$\boldsymbol{M}_0\ddot{\boldsymbol{d}}_0 + \boldsymbol{K}_0\boldsymbol{d}_0 = -\boldsymbol{\Gamma}_0 \tag{68}$$

$$\boldsymbol{M}_0\ddot{\boldsymbol{d}}_1 + \boldsymbol{K}_0\boldsymbol{d}_1 = -\boldsymbol{\Gamma}_1 - [2\omega_1\boldsymbol{M}_0 + \boldsymbol{M}_1]\ddot{\boldsymbol{d}}_0 - \boldsymbol{K}_1\boldsymbol{d}_0 \tag{69}$$

$$\boldsymbol{M}_0\ddot{\boldsymbol{d}}_2 + \boldsymbol{K}_0\boldsymbol{d}_2 = -\boldsymbol{\Gamma}_2 - [2\omega_1\boldsymbol{M}_0 + \boldsymbol{M}_1]\ddot{\boldsymbol{d}}_1 - \boldsymbol{K}_1\boldsymbol{d}_1 - \left[\left(2\omega_2 + \omega_1^2\right)\boldsymbol{M}_0 + 2\omega_1\boldsymbol{M}_1 + \boldsymbol{M}_2\right]\ddot{\boldsymbol{d}}_0 - \boldsymbol{K}_2\boldsymbol{d}_0 \tag{70}$$

which represent the asymptotic finite element equations of motion of the linear beam-string presented earlier.

Static Beam Results

When dynamic terms are neglected, the static shape modeling capability of this system can be evaluated. When the desired shape functions to this system are applied and the global stiffness matrices are compiled, for a desired grid, the beam's shape can be predicted by applying the following procedure:

$$\boldsymbol{d}_0 = -\boldsymbol{K}_0^{-1}\boldsymbol{\Gamma}_0 \tag{71}$$

$$\boldsymbol{d}_1 = -\boldsymbol{K}_0^{-1}[\boldsymbol{\Gamma}_1 + \boldsymbol{K}_1\boldsymbol{d}_0] \tag{72}$$

$$\boldsymbol{d}_2 = -\boldsymbol{K}_0^{-1}[\boldsymbol{\Gamma}_2 + \boldsymbol{K}_1\boldsymbol{d}_1 + \boldsymbol{K}_2\boldsymbol{d}_0] \tag{73}$$

$$\boldsymbol{d} = \boldsymbol{d}_0 + \varepsilon\boldsymbol{d}_1 + \varepsilon^2\boldsymbol{d}_2 \tag{74}$$

Each successive level of $\boldsymbol{d}_i$ corrects the fundamental $\boldsymbol{d}_0$ shape. Because each i level, $i = 1, \ldots, n$, is of the order of ε^i, the order of the system can be matched to the desired precision of the output. The displacements are directly affected by the choice of the shape functions. The shape function expansion developed in the Appendix satisfies the solvability conditions and can be used in this formulation.

The cubic beam string shape functions [Eq. (A7)] can now be employed. Figure 2 shows a selected result from applying a 10-element grid to a beam with same properties used in Table 1 and a thickness ratio of 0.006.

To see the significant improvement this method provides, in Figs. 3, the MIMS result error using cubic beam-string elements is compared to the standard finite element method error using standard C^1 elements. Both are measured against the analytical solution. Identical material properties and gridding were used. Although the standard model appears to produce a smoother result (because the bumps are an artifact of the method), the MIMS result is over three orders of magnitude more accurate. This error is representative of the accuracy limitation inherent in the standard method. Increasing the nodal density had no significant effect on the solution accuracy. Reducing the density ultimately reduced the accuracy of the standard solution, whereas the MIMS solution is capable of producing an accurate result with a single element due to the nature of the shape functions.

Table 1 Beam material properties

Property	Kapton	PVDF[a]
Young's modulus E, GPa	2.8	1.8
Thickness t^*, μm	16	8

[a]PVDF, polyvinylidine fluoride.

Dynamic Response

The dynamic properties of the clamped–clamped linear beam-string can be studied through the sequential evaluation of Eqs. (68–70). Forced response computation of a dynamic system often requires the addition of damping terms, but these terms cannot be directly inserted into the system Lagrangian. This effect is normally inserted directly into the equations of motion, and values are assigned through experimental evaluation. The MIMS will require a similar approach.

Finite element methods commonly model the damping term using the known mass and stiffness matrices. Rayleigh or proportional damping is one example[6]:

$$[\boldsymbol{C}] = \alpha^*[\boldsymbol{K}] + \beta^*[\boldsymbol{M}] \tag{75}$$

where α^* and β^* are related to critical damping ξ^* and frequency ω through

$$\xi^* = \tfrac{1}{2}(\alpha^*\omega + \beta^*/\omega) \tag{76}$$

The parameters α^* and β^* are considered $\mathcal{O}(\varepsilon)$ for the materials discussed herein.

To understand how the damping terms are related to the system presented in Eqs. (68–70), remove any temporal related scaling terms (dropping brackets [ ] again)

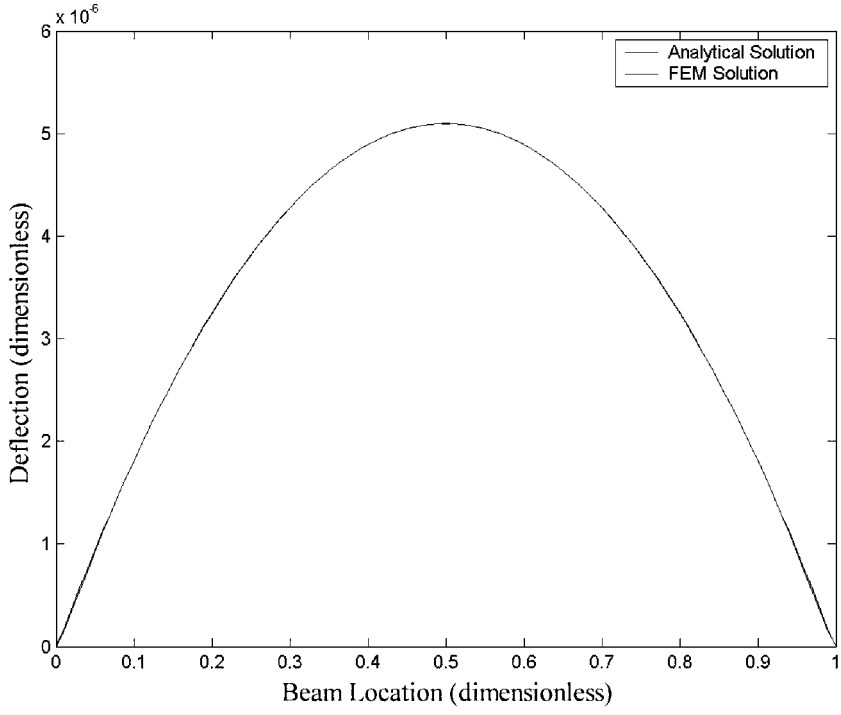

Fig. 2 Beam simulation using cubic beam-string elements.

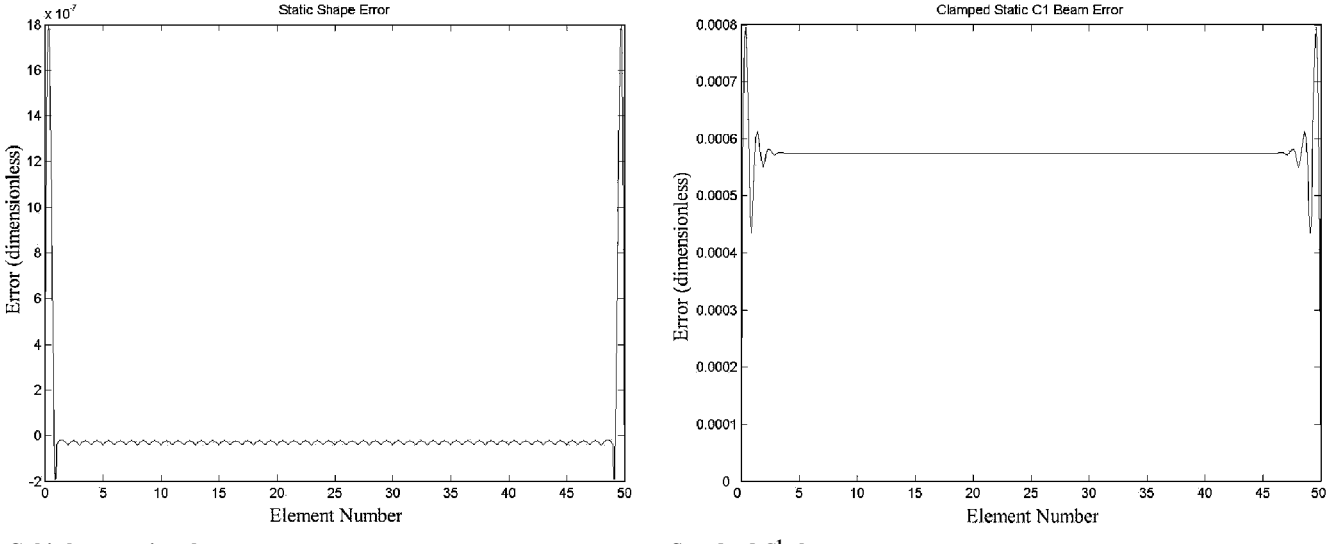

Cubic beam-string elements **Standard C^1 elements**

Fig. 3 Error comparison, 50 elements.

$$\boldsymbol{M}_0\ddot{\boldsymbol{d}}_0 + \boldsymbol{K}_0\boldsymbol{d}_0 = -\boldsymbol{\Gamma}_0 \tag{77}$$

$$\boldsymbol{M}_0\ddot{\boldsymbol{d}}_1 + \boldsymbol{K}_0\boldsymbol{d}_1 = -\boldsymbol{\Gamma}_1 - \boldsymbol{M}_1\ddot{\boldsymbol{d}}_0 - \boldsymbol{K}_1\boldsymbol{d}_0 \tag{78}$$

$$\boldsymbol{M}_0\ddot{\boldsymbol{d}}_2 + \boldsymbol{K}_0\boldsymbol{d}_2 = -\boldsymbol{\Gamma}_2 - \boldsymbol{M}_1\ddot{\boldsymbol{d}}_1 - \boldsymbol{K}_1\boldsymbol{d}_1 - \boldsymbol{M}_2\ddot{\boldsymbol{d}}_0 - \boldsymbol{K}_2\boldsymbol{d}_0 \tag{79}$$

When each level is multiplied by its corresponding ε order and the system is summed, the following results:

$$\boldsymbol{M}_0\sum_{i=0}^{n}\varepsilon^i\ddot{\boldsymbol{d}}_i + \boldsymbol{K}_0\sum_{i=0}^{n}\varepsilon^i\boldsymbol{d}_i = -\sum_{i=0}^{n}\varepsilon^i\boldsymbol{\Gamma}_i - \varepsilon\boldsymbol{M}_1\sum_{i=0}^{n-1}\varepsilon^i\ddot{\boldsymbol{d}}_i$$

$$-\varepsilon\boldsymbol{K}_1\sum_{i=0}^{n-1}\varepsilon^i\boldsymbol{d}_i - \varepsilon^2\boldsymbol{M}_2\sum_{i=0}^{n-2}\varepsilon^i\ddot{\boldsymbol{d}}_i - \varepsilon^2\boldsymbol{K}_2\sum_{i=0}^{n-2}\varepsilon^i\boldsymbol{d}_i - \cdots \tag{80}$$

Because $n \to \infty$, the system can be reorganized as

$$\boldsymbol{M}\ddot{\boldsymbol{d}} + \boldsymbol{K}\boldsymbol{d} = -\boldsymbol{\Gamma} \tag{81}$$

where

$$\boldsymbol{M} = \boldsymbol{M}_0 + \varepsilon\boldsymbol{M}_1 + \varepsilon^2\boldsymbol{M}_2 + \cdots$$

$$\boldsymbol{K} = \boldsymbol{K}_0 + \varepsilon\boldsymbol{K}_1 + \varepsilon^2\boldsymbol{K}_2 + \cdots$$

$$\boldsymbol{\Gamma} = \boldsymbol{\Gamma}_0 + \varepsilon\boldsymbol{\Gamma}_1 + \varepsilon^2\boldsymbol{\Gamma}_2 + \cdots$$

$$\boldsymbol{d} = \boldsymbol{d}_0 + \varepsilon\boldsymbol{d}_1 + \varepsilon^2\boldsymbol{d}_2 + \cdots \tag{82}$$

When this result is combined with Eq. (75), a damping matrix expansion is suggested:

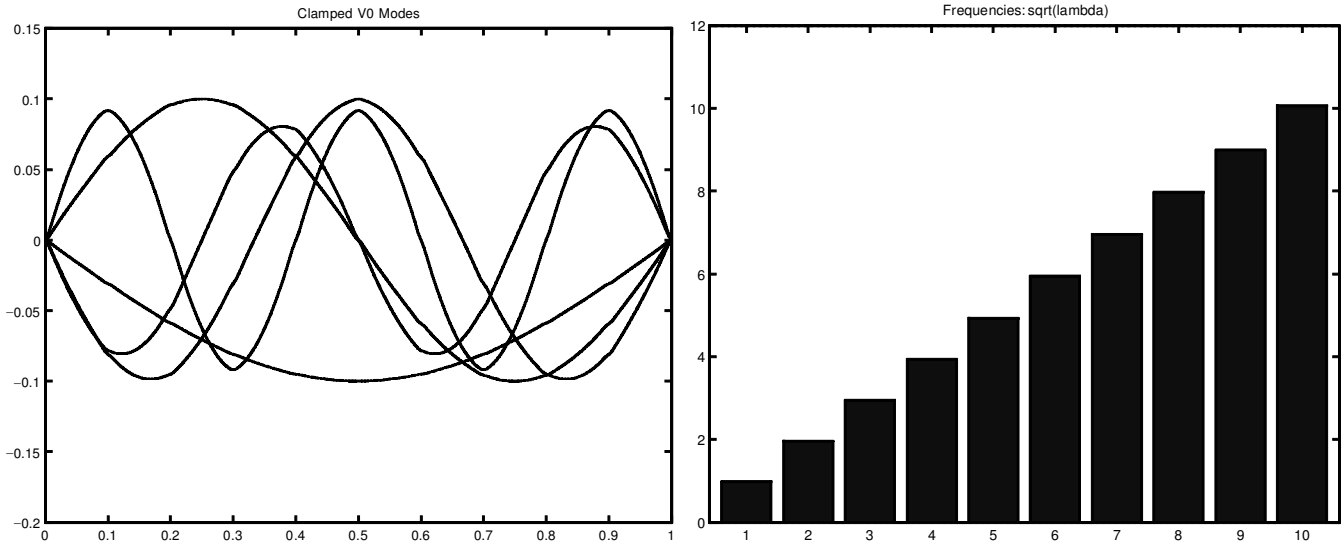

Fig. 4 Beam-string modes.

$$\boldsymbol{C} = \varepsilon \boldsymbol{C}_1 + \varepsilon^2 \boldsymbol{C}_2 + \cdots \tag{83}$$

where

$$\boldsymbol{C}_i = \alpha_1^* \boldsymbol{K}_{i-1} + \beta_1^* \boldsymbol{M}_{i-1} \tag{84}$$

This term can then be inserted into Eqs. (68–70), producing

$$\boldsymbol{M}_0 \ddot{\boldsymbol{d}}_0 + \boldsymbol{K}_0 \boldsymbol{d}_0 = -\boldsymbol{\Gamma}_0 \tag{85}$$

$$\boldsymbol{M}_0 \ddot{\boldsymbol{d}}_1 + \boldsymbol{K}_0 \boldsymbol{d}_1 = -\boldsymbol{\Gamma}_1 - [2\omega_1 \boldsymbol{M}_0 + \boldsymbol{M}_1]\ddot{\boldsymbol{d}}_0 - \boldsymbol{C}_1 \dot{\boldsymbol{d}}_0 - \boldsymbol{K}_1 \boldsymbol{d}_0 \tag{86}$$

$$\begin{aligned}\boldsymbol{M}_0 \ddot{\boldsymbol{d}}_2 + \boldsymbol{K}_0 \boldsymbol{d}_2 = {} & -\boldsymbol{\Gamma}_2 - [2\omega_1 \boldsymbol{M}_0 + \boldsymbol{M}_1]\ddot{\boldsymbol{d}}_1 - \boldsymbol{C}_1 \dot{\boldsymbol{d}}_1 - \boldsymbol{K}_1 \boldsymbol{d}_1 \\ & - \left[\left(2\omega_2 + \omega_1^2\right)\boldsymbol{M}_0 + 2\omega_1 \boldsymbol{M}_1 + \boldsymbol{M}_2\right]\ddot{\boldsymbol{d}}_0 - \boldsymbol{C}_2 \dot{\boldsymbol{d}}_0 - \boldsymbol{K}_2 \boldsymbol{d}_0\end{aligned} \tag{87}$$

The solution to Eq. (85) is found through a standard eigenanalysis method. When $\boldsymbol{d}_0 = \boldsymbol{\nu}_0 e^{i\omega_0 t}$ is assumed,

$$[\boldsymbol{K}_0 - \lambda_0 \boldsymbol{M}_0]\boldsymbol{\nu}_0 = 0 \tag{88}$$

where $\omega_0 = \sqrt{\lambda_0}$, the first-order frequencies of the system corresponding to the first-order mode shapes $\boldsymbol{\nu}_0$. When this methodology is continued to Eq. (86),

$$[\boldsymbol{K}_0 - \lambda_0 \boldsymbol{M}_0]\boldsymbol{\nu}_1 = -[\boldsymbol{K}_1 + i\omega_0 \boldsymbol{C}_1 - \lambda_0(2\omega_1 \boldsymbol{M}_0 + \boldsymbol{M}_1)]\boldsymbol{\nu}_0 \tag{89}$$

The space spanned by $\boldsymbol{\nu}_0$ completely defines all mode contributions allowed in Eq. (88). Any contribution to the solution through $\boldsymbol{\nu}_1$ must then be orthogonal to the $\boldsymbol{\nu}_0$ solution. We can impose this by premultiplying Eq. (89) by the solution of Eq. (88):

$$\boldsymbol{\nu}_0^T[\boldsymbol{K}_0 - \lambda_1 \boldsymbol{M}_0]\boldsymbol{\nu}_1 = -\boldsymbol{\nu}_0^T[\boldsymbol{K}_1 + i\omega_0 \boldsymbol{C}_1 - \lambda_0(2\omega_1 \boldsymbol{M}_0 + \boldsymbol{M}_1)]\boldsymbol{\nu}_0 \tag{90}$$

which results in only one undetermined value,

$$\omega_1 = \frac{\boldsymbol{\nu}_0^T[\boldsymbol{K}_1 + i\omega_0 \boldsymbol{C}_1 - \lambda_0 \boldsymbol{M}_1]\boldsymbol{\nu}_0}{2\lambda_0 \boldsymbol{\nu}_0^T \boldsymbol{M}_0 \boldsymbol{\nu}_0} \tag{91}$$

providing the first ω correction.

When this procedure is continued to the next level, the next ω correction can be calculated using the same procedure from Eq. (87):

$$\omega_2 = \frac{\boldsymbol{\nu}_0^T\left[\boldsymbol{K}_2 + i(\omega_0 \boldsymbol{C}_2 + \omega_1 \boldsymbol{C}_1) - \lambda_0\left(\omega_1^2 \boldsymbol{M}_0 + 2\omega_1 \boldsymbol{M}_1 + \boldsymbol{M}_2\right)\right]\boldsymbol{\nu}_0}{2\lambda_0 \boldsymbol{\nu}_0^T \boldsymbol{M}_0 \boldsymbol{\nu}_0} \tag{92}$$

The damped response frequencies can then be computed through Eq. (38).

With the dissipative terms neglected, Fig. 4 is a plot of the first five computed wave shapes predicted by this system and the scaled mode frequencies. As the beam's thickness-to-length ratio decreases, the scaled modal frequencies continue to approach integer values representing string solutions.[7]

This method produces excellent results when applied to the linear beam-string model. Perturbation methods, in general, are most valuable as tools to tackle more complicated nonlinear problems. In the next section, a nonlinear problem is attacked.

Nonlinear Laminated Piezothermoelastic Beam-String

Formulation

The nonlinear piezoelectric laminated beam analytically solved by Rogers and Agnes[1] can be analyzed using a finite element approach based on the presented MIMS. The Lagrangian for this beam is

$$\begin{aligned}\hat{\mathbb{L}} = \int_{\hat{\mathcal{V}}} \Bigg[& \frac{1}{2}\rho\left(\hat{u}_{,\hat{t}}^2 + \hat{w}_{,\hat{t}}^2\right) - \frac{1}{2}E\left(\hat{u}_{,\hat{x}} + \frac{1}{2}\hat{w}_{,\hat{x}}^2 + \frac{1}{2}\hat{u}_{,\hat{x}}\hat{w}_{,\hat{x}}^2 - \frac{1}{8}\hat{w}_{,\hat{x}}^4\right)^2 \\ & - E\hat{z}^2\hat{w}_{,\hat{x}\hat{x}}^2 + E\epsilon_0 z\hat{w}_{,\hat{x}\hat{x}} + E\hat{z}\hat{w}_{,\hat{x}\hat{x}}\left(\hat{u}_{,\hat{x}} + \frac{1}{2}\hat{w}_{,\hat{x}}^2 + \frac{1}{2}\hat{u}_{,\hat{x}}\hat{w}_{,\hat{x}}^2 \right. \\ & \left. - \frac{1}{8}\hat{w}_{,\hat{x}}^4\right) - E\epsilon_0\left(\hat{u}_{,\hat{x}} + \frac{1}{2}\hat{w}_{,\hat{x}}^2 + \frac{1}{2}\hat{u}_{,\hat{x}}\hat{w}_{,\hat{x}}^2 - \frac{1}{8}\hat{w}_{,\hat{x}}^4\right) \\ & + \frac{N_0}{A}\left(\hat{u}_{,\hat{x}} + \frac{1}{2}\hat{w}_{,\hat{x}}^2 + \frac{1}{2}\hat{u}_{,\hat{x}}\hat{w}_{,\hat{x}}^2 - \frac{1}{8}\hat{w}_{,\hat{x}}^4\right) - \frac{N_0}{A}\hat{z}\hat{w}_{,\hat{x}\hat{x}}\Bigg] \mathrm{d}\hat{\mathcal{V}} \\ & + \int_{\hat{x}} \hat{P}\left(\hat{w} + \hat{u}_{,\hat{x}}\hat{w} - \hat{w}_{,\hat{x}}\hat{u}\right)\mathrm{d}\hat{x}\end{aligned} \tag{93}$$

where

$$\epsilon_0 = d_{31} V \big/ t^* + \bar{\alpha} T \tag{94}$$

Note that Eq. (93) differs from Eq. (5) because it includes nonlinear terms.

To reduce this system to a one-dimensional beam representation, the following parameters are defined:

$$\rho A = \int_A \rho \, \mathrm{d}A, \qquad N_z = \int_A \frac{N_i}{A} z \, \mathrm{d}A, \qquad EA = \int_A E \, \mathrm{d}A$$

$$N_0 = \int_A \frac{N_i}{A} \, \mathrm{d}A, \qquad EA_\epsilon = \int_A E\epsilon_0 \, \mathrm{d}A, \qquad EA_{\epsilon z} = \int_A E\epsilon_0 \hat{z} \, \mathrm{d}A$$

$$EI = \int_A E\hat{z}^2 \, \mathrm{d}A, \qquad EA_z = \int_A E\hat{z} \, \mathrm{d}A \tag{95}$$

If all measurements are with respect to the original neutral axis of a symmetric laminate, N_z and EA_z are trivial. To properly perform the MIMS procedure, the system must be put in nondimensional form. The following nondimensional parameter scaling rules were used:

$$x = \frac{\hat{x}}{L}, \qquad z = \frac{\hat{z}}{L}, \qquad u = \frac{\hat{u}}{L}, \qquad w = \frac{\hat{w}}{L}, \qquad r^2 = \frac{EI}{L^2 EA}\eta$$

$$P = \frac{\hat{P}L}{EA}\eta, \qquad N_0 = \frac{1}{\eta}, \qquad N_z = \frac{N_z}{LEA}\eta, \qquad EA_z = \frac{EA_z}{LEA}\eta$$

$$EA_{\epsilon z} = \frac{EA_{\epsilon z}}{LEA}\eta, \qquad EA_\epsilon = \frac{EA_\epsilon}{EA}\eta, \qquad t^2 = \frac{c_2^2}{L^2}\hat{t}^2$$

where $\eta = c_1^2/c_2^2$ and $c_1 = \sqrt{(EA/\rho A)}$ and $c_2 = \sqrt{(N_0/\rho A)}$ are the longitudinal and transverse speeds of sound in the beam. The resulting scaled nonlinear laminated piezothermoelastic beam's Lagrangian is

$$\begin{aligned}\mathbb{L} = \int_0^1 & \frac{1}{2}\left(u_{,t}^2 + w_{,t}^2\right) - \frac{1}{2}\eta_{-1}\left(u_{,x} + \frac{1}{2}w_{,x}^2 + \frac{1}{2}u_{,x}w_{,x}^2 - \frac{1}{8}w_{,x}^4\right)^2 \\ & - \varepsilon^2 w_{,xx}^2 + EZ_2 w_{,xx}\left(u_{,x} + \frac{1}{2}w_{,x}^2 + \frac{1}{2}u_{,x}w_{,x}^2 - \frac{1}{8}w_{,x}^4\right) \\ & + EZ_{\epsilon 3} w_{,xx} - N_z w_{,xx} - (1 - EA_{\epsilon 2})\left(u_{,x} + \frac{1}{2}w_{,x}^2\right. \\ & \left. + \frac{1}{2}u_{,x}w_{,x}^2 - \frac{1}{8}w_{,x}^4\right) + P_2(w + u_{,x}w - w_{,x}u)\,\mathrm{d}x\end{aligned} \tag{96}$$

where the subscript numbering indicates the specific parameter's relative order based on the order of ε. With the correctly scaled Lagrangian available, MIMS can now be applied.

The boundary-layer areas are introduced through the stretching variables (or spatial scales)

$$u(x,t) \to u(\eta, \xi, \zeta, t; \varepsilon), \qquad w(x,t) \to w(\eta, \xi, \zeta, t; \varepsilon) \tag{97}$$

where $\eta = x$, $\xi = x/\varepsilon$, and $\zeta = (1-x)/\varepsilon$. When Eqs. (14) and (15) are applied along with the expansions (and temporal scaling is introduced)

$$T_n = \varepsilon^n \tau \tag{98}$$

$$t = \omega\tau \tag{99}$$

$$\omega = \omega_0 + \varepsilon\omega_1 + \varepsilon^2\omega_2 + \cdots \tag{100}$$

$$\boldsymbol{N}(\eta, \xi, \zeta; \varepsilon) = \boldsymbol{N}_0(\eta, \xi, \zeta) + \varepsilon\boldsymbol{N}_1(\eta, \xi, \zeta) + \cdots \tag{101}$$

$$\boldsymbol{N}_u(\eta, \xi, \zeta; \varepsilon) = \boldsymbol{N}_{u0}(\eta, \xi, \zeta) + \varepsilon\boldsymbol{N}_{u1}(\eta, \xi, \zeta) + \cdots \tag{102}$$

$$\boldsymbol{d}(t; \varepsilon) = \varepsilon^2\boldsymbol{d}_2(t) + \varepsilon^3\boldsymbol{d}_3(t) + \varepsilon^4\boldsymbol{d}_4(t) + \cdots \tag{103}$$

$$\boldsymbol{d}_u(t; \varepsilon) = \varepsilon^3\boldsymbol{d}_{u3}(t) + \varepsilon^4\boldsymbol{d}_{u4}(t) + \varepsilon^5\boldsymbol{d}_{u5}(t) + \cdots \tag{104}$$

$$u(\eta, \xi, \zeta, t; \varepsilon) = \boldsymbol{N}_u(\eta, \xi, \zeta; \varepsilon)\boldsymbol{d}_u(t; \varepsilon) \tag{105}$$

$$w(\eta, \xi, \zeta, t; \varepsilon) = \boldsymbol{N}(\eta, \xi, \zeta; \varepsilon)\boldsymbol{d}(t; \varepsilon) \tag{106}$$

where $\omega_0 = 1$, because the original system was effectively scaled by ω_0, into Eq. (97) produces a multiple scales Lagrangian expansion. Separating the resulting expansion into ε-order groupings produces a set of Lagrangians of increasing order, or the Lagrangian expansion

$$\mathbb{L} = \varepsilon^{-2}\mathbb{L}_{-2} + \varepsilon^{-1}\mathbb{L}_{-1} + \mathbb{L}_0 + \varepsilon\mathbb{L}_1 + \varepsilon^2\mathbb{L}_2 + \cdots \tag{107}$$

Once again, selecting the order of precision is equivalent to selecting an element in the energy expansion. Applying Euler's equations to the selected Lagrangian element produces the system of equations that will produce the desired solution. The functions produced through the application of Euler's equations to $\mathbb{L}_n$ exists in the set of functions produced through the application of Euler's equations to $\mathbb{L}_m$, where $m > n$.

Applying Euler's equations to $\mathbb{L}_2$ produces the following decoupled system of equations:

$$\boldsymbol{K}_{-2}\boldsymbol{d}_2 = 0 \tag{108}$$

$$\boldsymbol{K}_{-2}\boldsymbol{d}_3 = -\boldsymbol{K}_{-1}\boldsymbol{d}_2 \tag{109}$$

$$\boldsymbol{K}_{-2}\boldsymbol{d}_4 = -\boldsymbol{K}_{-1}\boldsymbol{d}_3 - \boldsymbol{\Gamma}_0 - \boldsymbol{M}_0\boldsymbol{d}_{3,00} - \boldsymbol{K}_0\boldsymbol{d}_0 \tag{110}$$

$$\begin{aligned}\boldsymbol{K}_{-2}\boldsymbol{d}_5 = & -\boldsymbol{K}_{-1}\boldsymbol{d}_4 - \boldsymbol{\Gamma}_1 - \boldsymbol{M}_0\boldsymbol{d}_{4,00} - \boldsymbol{K}_0\boldsymbol{d}_3 \\ & - 2\boldsymbol{M}_0(\omega_1\boldsymbol{d}_{0,00} + \boldsymbol{d}_{0,01}) - \boldsymbol{M}_1\boldsymbol{d}_{0,00} - \boldsymbol{K}_1\boldsymbol{d}_0\end{aligned} \tag{111}$$

$$\begin{aligned}\boldsymbol{K}_{-2}\boldsymbol{d}_6 = & -\boldsymbol{K}_{-1}\boldsymbol{d}_5 - \boldsymbol{\Gamma}_2 - \boldsymbol{M}_0\boldsymbol{d}_{5,00} - \boldsymbol{K}_0\boldsymbol{d}_3 \\ & - 2\boldsymbol{M}_0(\omega_1\boldsymbol{d}_{3,00} + \boldsymbol{d}_{3,01}) - \boldsymbol{M}_1\boldsymbol{d}_{3,00} - \boldsymbol{K}_1\boldsymbol{d}_3 \\ & - \boldsymbol{M}_0\left[\boldsymbol{d}_{2,11} + \boldsymbol{d}_{2,02} + 4\omega_1\boldsymbol{d}_{2,01} + \left(\omega_1^2 + 2\omega_2\right)\boldsymbol{d}_{2,00}\right] \\ & - 2\boldsymbol{M}_1(\omega_1\boldsymbol{d}_{2,00} + \boldsymbol{d}_{2,01}) - \boldsymbol{M}_2\boldsymbol{d}_{2,00} - \boldsymbol{K}_2\boldsymbol{d}_2\end{aligned} \tag{112}$$

$$\boldsymbol{M}_{u0}\boldsymbol{d}_{u3,00} = 0 \tag{113}$$

where $\boldsymbol{K}_i$ are system stiffness matrices, $\boldsymbol{M}_i$ and $\boldsymbol{M}_{u0}$ are system mass matrices, and $\boldsymbol{\Gamma}_i$ are system forcing. Additional equations of import are

$$\begin{aligned}\boldsymbol{N}_{u3,\xi} &= \boldsymbol{N}_{u3,\zeta}, & \boldsymbol{N}_{u4,\xi} &= \boldsymbol{N}_{u4,\zeta} \\ \boldsymbol{N}_{u5,\xi} &= \boldsymbol{N}_{u5,\zeta}, & \boldsymbol{N}_{u6,\xi} &= \boldsymbol{N}_{u6,\zeta}\end{aligned} \tag{114}$$

Equations (108) and (109) are the first two solvability equations. These drive the choice of shape functions necessary. Equations (114) presents an additional set of solvability conditions in this analysis. These indicate no axial boundary-layer effects exist, to this level, based on the assumptions and scaling choices made earlier in this analysis. Additionally, the axial displacements are not present in the transverse displacement equations at the level of expansion presented. Therefore, the axial displacements will not be considered in the remaining portion of this beam analysis.

The various system matrices can be calculated by applying either of the shape functions presented in the Appendix. The resulting matrices are

$$\boldsymbol{K}_{-2} = 0, \qquad \boldsymbol{K}_{-1} = 0, \qquad \boldsymbol{K}_0 = \int_x \boldsymbol{F}_1^T\boldsymbol{F}_1 + \boldsymbol{G}_1^T\boldsymbol{G}_1 \, \mathrm{d}x$$

$$\boldsymbol{K}_1 = \int_x \boldsymbol{F}_1^T\boldsymbol{F}_2 + \boldsymbol{F}_2^T\boldsymbol{F}_1 + \boldsymbol{G}_1^T\boldsymbol{G}_2 + \boldsymbol{G}_2^T\boldsymbol{G}_1 \, \mathrm{d}x$$

$$\begin{aligned}\boldsymbol{K}_2 = \int_x & \boldsymbol{F}_2^T\boldsymbol{F}_2 + \boldsymbol{F}_1^T\boldsymbol{F}_3 + \boldsymbol{F}_3^T\boldsymbol{F}_1 + \boldsymbol{G}_2^T\boldsymbol{G}_2 + \boldsymbol{G}_1^T\boldsymbol{G}_3 \\ & + \boldsymbol{G}_3^T\boldsymbol{G}_1 + EA_{\epsilon 2}\boldsymbol{G}_1^T\boldsymbol{G}_1 \, \mathrm{d}x\end{aligned} \tag{115}$$

$$\boldsymbol{M}_0 = \int_x \boldsymbol{N}_0^T \boldsymbol{N}_0 \, \mathrm{d}x, \qquad \boldsymbol{M}_1 = \int_x \boldsymbol{N}_0^T \boldsymbol{N}_1 + \boldsymbol{N}_1^T \boldsymbol{N}_0 \, \mathrm{d}x$$

$$\boldsymbol{M}_2 = \int_x \boldsymbol{N}_1^T \boldsymbol{N}_1 + \boldsymbol{N}_0^T \boldsymbol{N}_2 + \boldsymbol{N}_2^T \boldsymbol{N}_0 \, \mathrm{d}x \tag{116}$$

The forcing vectors are similarly produced:

$$\boldsymbol{\Gamma}_0 = \int_x -P\boldsymbol{N}_0^T \, \mathrm{d}x, \qquad \boldsymbol{\Gamma}_1 = \int_x (N_{z3} - EZ_{\epsilon 3})\boldsymbol{F}_1^T - P\boldsymbol{N}_1^T \, \mathrm{d}x$$

$$\boldsymbol{\Gamma}_2 = \int_x (N_{z3} - EZ_{\epsilon 3})\boldsymbol{F}_2^T - P\boldsymbol{N}_2^T \, \mathrm{d}x \tag{117}$$

The actuation manifests itself through an axial strain term $EA_{\epsilon 2}$ and a boundary moment term $EZ_{\epsilon 3}$. The axial term modifies the system stiffness, and the boundary term acts as an applied forcing term. The multiple scales integral [Eq. (51)] is used here again without modification.

The undamped dynamic system of equations is then

$$\boldsymbol{M}_0\boldsymbol{d}_{2,00} + \boldsymbol{K}_0\boldsymbol{d}_2 = -\boldsymbol{\Gamma}_0 \tag{118}$$

$$\boldsymbol{M}_0\boldsymbol{d}_{3,00} + \boldsymbol{K}_0\boldsymbol{d}_3 = -\boldsymbol{\Gamma}_1 - (2\omega_1\boldsymbol{M}_0 + \boldsymbol{M}_1)\boldsymbol{d}_{2,00} - 2\boldsymbol{M}_0\boldsymbol{d}_{2,01} - \boldsymbol{K}_1\boldsymbol{d}_2 \tag{119}$$

$$\boldsymbol{M}_0\boldsymbol{d}_{4,00} + \boldsymbol{K}_0\boldsymbol{d}_4 = -\boldsymbol{\Gamma}_2 - (2\omega_1\boldsymbol{M}_0 + \boldsymbol{M}_1)\boldsymbol{d}_{3,00} - 2\boldsymbol{M}_0\boldsymbol{d}_{3,01} - \boldsymbol{K}_1\boldsymbol{d}_3 - \left[\left(\omega_1^2 + 2\omega_2\right)\boldsymbol{M}_0 + 2\omega_1\boldsymbol{M}_1 + \boldsymbol{M}_2\right]\boldsymbol{d}_{2,00} - 2(2\omega_1\boldsymbol{M}_0 + \boldsymbol{M}_1)\boldsymbol{d}_{2,01} - \boldsymbol{M}_0\boldsymbol{d}_{2,11} - 2\boldsymbol{M}_0\boldsymbol{d}_{2,02} - \boldsymbol{K}_2\boldsymbol{d}_2 \tag{120}$$

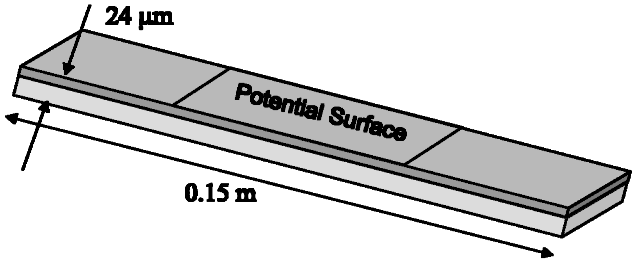

Fig. 5 Laminated piezothermoelastic beam configuration.

which represents the finite element equations of motion of the nonlinear laminated piezothermoelastic beam string. Including damping terms results in the damped dynamic system of equations for a nonlinear piezoelectric beam-string:

$$\boldsymbol{M}_0\boldsymbol{d}_{2,00} + \boldsymbol{K}_0\boldsymbol{d}_2 = -\boldsymbol{\Gamma}_0 \tag{121}$$

$$\boldsymbol{M}_0\boldsymbol{d}_{3,00} + \boldsymbol{K}_0\boldsymbol{d}_3 = -\boldsymbol{\Gamma}_1 - (2\omega_1\boldsymbol{M}_0 + \boldsymbol{M}_1)\boldsymbol{d}_{2,00} - 2\boldsymbol{M}_0\boldsymbol{d}_{2,01} - \boldsymbol{C}_1\boldsymbol{d}_{2,0} - \boldsymbol{K}_1\boldsymbol{d}_2 \tag{122}$$

$$\boldsymbol{M}_0\boldsymbol{d}_{4,00} + \boldsymbol{K}_0\boldsymbol{d}_4 = -\boldsymbol{\Gamma}_2 - (2\omega_1\boldsymbol{M}_0 + \boldsymbol{M}_1)\boldsymbol{d}_{3,00} - 2\boldsymbol{M}_0\boldsymbol{d}_{3,01} - \boldsymbol{C}_1\boldsymbol{d}_{3,0} - \boldsymbol{K}_1\boldsymbol{d}_3 - \left[\left(\omega_1^2 + 2\omega_2\right)\boldsymbol{M}_0 + 2\omega_1\boldsymbol{M}_1 + \boldsymbol{M}_2\right]\boldsymbol{d}_{2,00} - 2\boldsymbol{M}_0\boldsymbol{d}_{2,02} - 2(2\omega_1\boldsymbol{M}_0 + \boldsymbol{M}_1)\boldsymbol{d}_{2,01} - \boldsymbol{M}_0\boldsymbol{d}_{2,11} - \boldsymbol{C}_2\boldsymbol{d}_{2,0} - \boldsymbol{C}_1\boldsymbol{d}_{2,1} - \boldsymbol{K}_2\boldsymbol{d}_2 \tag{123}$$

Additional effects can be introduced with increasing Lagrangian order selection. This system can now be used to analyze problem solutions unattainable through analytical methods. Each level is solved in succession to produce an increasingly more accurate prediction.

Results

A piezoelastic laminated beam shown in Fig. 5 was modeled with the properties listed in Table 1. When an etched electrode covering the center third of the beam is used, the shape presented in Fig. 6 results from only electrical potential application ($d_{31}V = 10^{-7}$). Each plot is the result of successive solution orders. There is no deflection from the first-order solution due to the lack of any forcing term at that level. Notice the significant change in shape through the two subsequent orders. The second-order solution provides initial peizomoments, whereas the third-order solution corrects the result through the additional axial forcing terms.

The electrical interface regions are of particular interest. Modeling these regions of step changes with standard finite elements requires significant grid density increases near these areas. These standard modeling techniques are required to avoid the singularities existing in this region. The method presented here seems to overcome this problem and produces results more closely aligned with experimental observations.

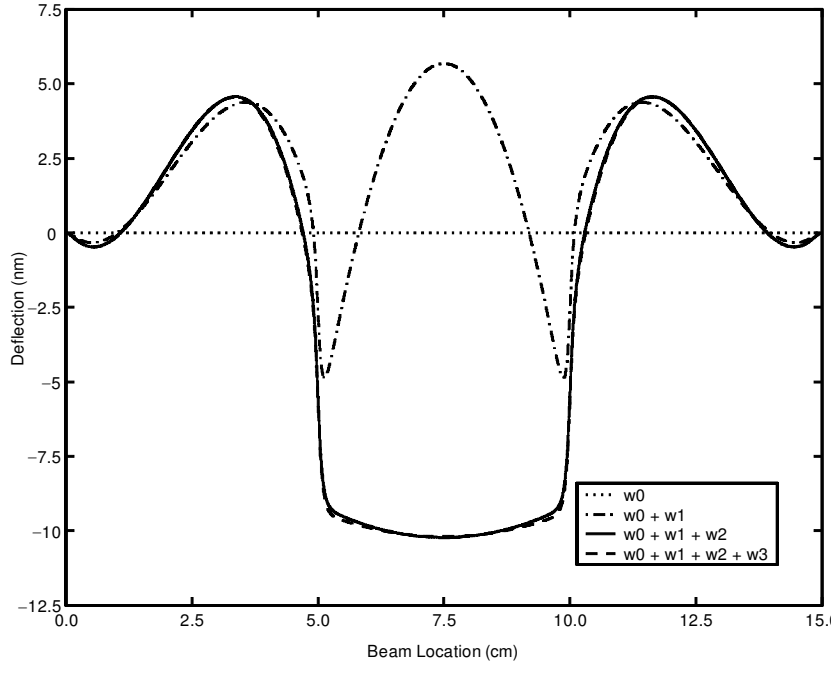

Fig. 6 Piezoelastic laminated beam corrections.

Conclusions

The MIMS was introduced and used to create an asymptotic finite element approach. By the use of a new set of parametric shape functions based on beam strings developed in the Appendix, the utility of this method was revealed. Applying these shape functions to a linear beam-string model in both static and dynamic analysis indicated the supremacy of the asymptotic set.

To further illustrate its utility, a nonlinear laminated beam was analyzed. The new method combines the utility of perturbation methods with the flexibility of finite element methods allowing for efficient solutions of nonlinear structural systems.

The use of the cubic beam-string shape functions in the MIMS asymptotic finite element method resulted in extremely high precision and, thus, provides a methodology that could provide a more efficient analytical tool for the development of inflatable structures.

Appendix: Functions

Asymptotic Shape

Application of the finite element method to a given problem is a balance between required output precision and available computational resources. The finite element method involves substituting an assumed shape function/unknown displacement pair for all dependent variables to be approximated. The simple one-dimensional string or rod model may use C^0 elements because the functions defining their motion are functions of only displacement. An example of a C^0 shape function vector is[6]

$$\boldsymbol{N}(x)^T = \begin{bmatrix} x/L \\ (L-x)/L \end{bmatrix} \tag{A1}$$

The linear nature of this function means that values are linearly interpolated. Elements created from this class of shape functions are unable to model nodal slopes, but may produce adequate results through postprocessing adjustments. C^0 elements, however, are not adequate if the essential boundary conditions include the displacement's derivatives. More complicated C^1 shape functions can be applied, but increase element matrix size, and therefore, computational speed can dramatically decrease. An example of a standard C^1 shape function vector is[6]

$$\boldsymbol{N}(x)^T = \begin{pmatrix} 1 - \dfrac{3x^2}{L^2} + \dfrac{2x^3}{L^3} \\ x - \dfrac{2x^2}{L} + \dfrac{x^3}{L^2} \\ \dfrac{3x^2}{L^2} - \dfrac{2x^3}{L^3} \\ -\dfrac{x^2}{L} + \dfrac{x^3}{L^2} \end{pmatrix} \tag{A2}$$

A beam-string solution requires C^1 class shape functions but is far too flexible and can exhibit locking problems when bending stiffness becomes very small. To provide a better solution method, elements that behave as beam strings can represent an extremely flexible structure. A beam string, however, does not produce a solution with curvature away from the boundary regions. It was also found that by adding an internal node, thereby allowing some internal curvature, a set of asymptotic shape functions could be created that can be used to model efficiently a highly compliant beam-string element.

Cubic Beam-String Shape

When an internal node is placed at the half-way point, a simple beam string of unit length with smallness parameter ε can be defined by the scaled static equation of motion

$$\varepsilon^2 \frac{\mathrm{d}^4 N}{\mathrm{d}x^4} - \frac{\mathrm{d}^2 N}{\mathrm{d}x^2} = 0 \tag{A3}$$

Table A1 Cubic beam-string shape function boundary conditions

	Shape function boundary condition					
	$w(0)$	$w_{,x}(0)$	$w(1)$	$w_{,x}(1)$	$w(1/2)$	$w_{,x}(1/2)$
Load	α	β	γ	δ	ψ	ϕ
N_1	1	0	0	0	0	0
N_2	0	1	0	0	0	0
N_3	0	0	1	0	0	0
N_4	0	0	0	1	0	0
N_5	0	0	0	0	1	0
N_6	0	0	0	0	0	1

with boundary conditions

$$N(0) = \alpha, \qquad N(1) = \gamma, \qquad N\left(\frac{1}{2}\right) = \psi$$

$$\left.\frac{\mathrm{d}N}{\mathrm{d}x}\right|_{x=0} = \beta, \qquad \left.\frac{\mathrm{d}N}{\mathrm{d}x}\right|_{x=1} = \delta, \qquad \left.\frac{\mathrm{d}N}{\mathrm{d}x}\right|_{x=\frac{1}{2}} = \phi \tag{A4}$$

The outer and inner solutions have the form

$$N^o(\eta) = \sum_{i=0}^{n} \varepsilon^i \left[a_{i0} + a_{i1}\eta + a_{i2}\eta^2 + a_{i3}\eta^3\right]$$

$$N^i(\xi) = \sum_{i=0}^{n} \varepsilon^i \left[b_{i0} + b_{i1}\xi + b_{i2}e^{-\xi}\right]$$

$$N^I(\zeta) = \sum_{i=0}^{n} \varepsilon^i \left[c_{i0} + c_{i1}\zeta + c_{i2}e^{-\zeta}\right] \tag{A5}$$

with boundary conditions outlined in Table A1, where $\eta = x$, $\xi = x/\varepsilon$, and $\zeta = (1-x)/\varepsilon$. Applying boundary conditions to the inner solutions then matching to the outer solutions of each order i in succession results in the following asymptotic beam-string solution:

$$\begin{aligned}
N(\eta, \xi, \zeta; \hat{\varepsilon}) &= \alpha + (\gamma - 5\alpha + 4\psi - 2\phi)\eta \\
&\quad + (8\alpha - 4\gamma - 4\psi + 6\phi)\eta^2 + (4\gamma - 4\alpha - 4\phi)\eta^3 \\
&\quad + \varepsilon[(5\alpha - \gamma + \beta - 4\psi + 2\phi) \\
&\quad + (10\gamma - 26\alpha - 5\beta - \delta + 16\psi - 12\phi)\eta \\
&\quad + (44\alpha - 28\gamma + 8\beta + 4\delta - 16\psi + 24\phi)\eta^2 \\
&\quad + (24\gamma - 24\alpha - 4\beta - 4\delta - 16\phi)\eta^3 \\
&\quad + (\gamma - 5\alpha - \beta + 4\psi - 2\phi)e^{-\xi} \\
&\quad + (\alpha - 5\gamma + \delta + 4\psi + 2\phi)e^{-\zeta}] \\
&\quad + \varepsilon^2[(26\alpha - 5\gamma + 5\beta + \delta - 16\psi + 12\phi) \\
&\quad + (76\gamma - 140\alpha - 26\beta - 10\delta + 64\psi - 72\phi)\eta \\
&\quad + (248\alpha - 184\gamma + 44\beta + 28\delta - 64\psi + 144\phi)\eta^2 \\
&\quad + (144\gamma - 144\alpha - 24\beta - 24\delta - 96\phi)\eta^3 \\
&\quad + (10\gamma - 26\alpha - 5\beta - \delta + 16\psi - 12\phi)e^{-\xi} \\
&\quad + (10\alpha - 26\gamma + 5\delta + \beta + 16\psi + 12\phi)e^{-\zeta}] \\
&\quad + \varepsilon^3[(140\alpha - 76\gamma + 26\beta + 10\delta - 64\psi + 72\phi) \\
&\quad + (520\gamma - 776\alpha - 140\beta - 76\delta + 256\psi - 432\phi)\eta \\
&\quad + (1424\alpha - 1168\gamma + 248\beta + 184\delta - 256\psi + 864\phi)\eta^2 \\
&\quad + (864\gamma - 864\alpha - 144\beta - 144\delta - 576\phi)\eta^3
\end{aligned}$$

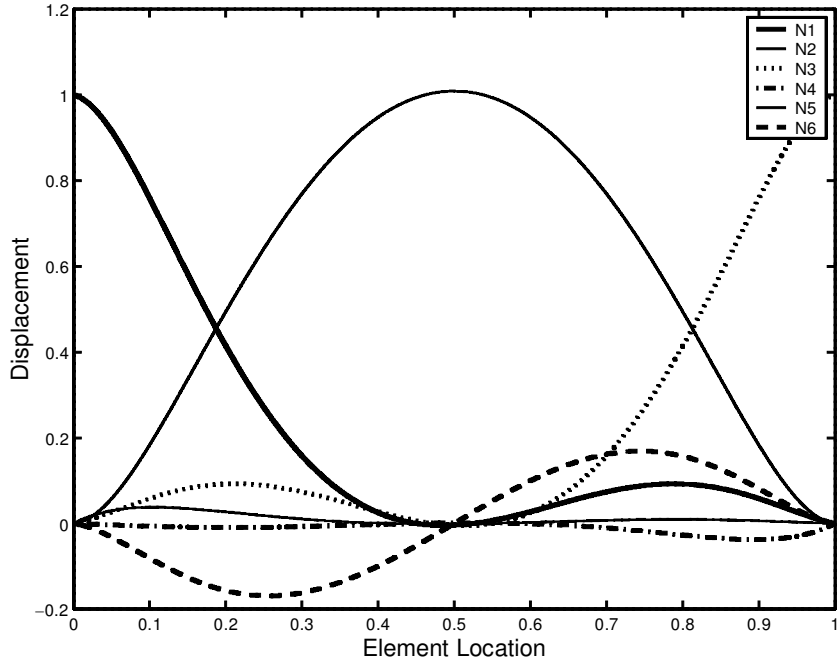

Fig. A1 Cubic beam-string shape functions, $\varepsilon = 0.1$.

$$+(76\gamma - 140\alpha - 26\beta - 10\delta + 64\psi - 72\phi)e^{-\xi}$$
$$+(76\alpha - 140\gamma + 26\delta + 10\beta + 64\psi + 72\phi)e^{-\zeta}]$$
$$+\mathcal{O}(\varepsilon^3) \tag{A6}$$

where

$$\alpha = w(0), \qquad \gamma = w(1), \qquad \psi = w\left(\tfrac{1}{2}\right)$$

$$\beta = w_{,x}(0), \qquad \delta = w_{,x}(1), \qquad \phi = w_{,x}\left(\tfrac{1}{2}\right)$$

Applying the boundary conditions in Table A1 to Eq. (A6) produces the following shape function vector:

$$N^T = \begin{pmatrix} N_1 \\ N_2 \\ N_3 \\ N_4 \\ N_5 \\ N_6 \end{pmatrix} = \begin{pmatrix} 1 - 5\eta + 8\eta^2 - 4\eta^3 \\ 0 \\ \eta - 4\eta^2 + 4\eta^3 \\ 0 \\ 4\eta - 4\eta^2 \\ -2\eta + 6\eta^2 - 4\eta^3 \end{pmatrix}$$

$$+\varepsilon \begin{pmatrix} 5 - 26\eta + 44\eta^2 - 24\eta^3 - 5e^{-\xi} + e^{-\zeta} \\ 1 - 5\eta + 8\eta^2 - 4\eta^3 - e^{-\xi} \\ -1 + 10\eta - 28\eta^2 + 24\eta^3 + e^{-\xi} - 5e^{-\zeta} \\ -\eta + 4\eta^2 - 4\eta^3 + e^{-\zeta} \\ -4 + 16\eta - 16\eta^2 + 4e^{-\xi} + 4e^{-\zeta} \\ 2 - 12\eta + 24\eta^2 - 16\eta^3 - 2e^{-\xi} + 2e^{-\zeta} \end{pmatrix}$$

$$+\varepsilon^2 \begin{pmatrix} 26 - 140\eta + 248\eta^2 - 144\eta^3 - 26e^{-\xi} + 10e^{-\zeta} \\ 5 - 26\eta + 44\eta^2 - 24\eta^3 - 5e^{-\xi} + e^{-\zeta} \\ -10 + 76\eta - 184\eta^2 + 144\eta^3 + 10e^{-\xi} - 26e^{-\zeta} \\ 1 - 10\eta + 28\eta^2 - 24\eta^3 - e^{-\xi} + 5e^{-\zeta} \\ -16 + 64\eta - 64\eta^2 + 16e^{-\xi} + 16e^{-\zeta} \\ 12 - 72\eta + 144\eta^2 - 96\eta^3 - 12e^{-\xi} + 12e^{-\zeta} \end{pmatrix}$$

$$+\varepsilon^3 \begin{pmatrix} 140 - 776\eta + 1424\eta^2 - 864\eta^3 - 140e^{-\xi} + 76e^{-\zeta} \\ 26 - 140\eta + 248\eta^2 - 144\eta^3 - 26e^{-\xi} + 10e^{-\zeta} \\ -76 + 520\eta - 1168\eta^2 + 864\eta^3 + 76e^{-\xi} - 140e^{-\zeta} \\ 10 - 76\eta + 184\eta^2 - 144\eta^3 - 10e^{-\xi} + 26e^{-\zeta} \\ -64 + 256\eta - 256\eta^2 + 64e^{-\xi} + 64e^{-\zeta} \\ 72 - 432\eta + 864\eta^2 - 576\eta^3 - 72e^{-\xi} + 72e^{-\zeta} \end{pmatrix}$$
$$+\mathcal{O}(\varepsilon^4) \tag{A7}$$

Figure A1 shows the behavior of these shape functions. The shape functions are as a result of selecting an ε value 0.1. This element can support nodal slopes and allows some curvature away from the boundary. Also note that the shape functions themselves are expansions in orders of ε, which can be included early in a perturbation finite element development.

Acknowledgments

This work was supported by the Air Force Office of Scientific Research, Brian Sanders and Daniel Segalman monitoring. Additionally, we thank William Baker for his insights and suggestions throughout the development of this material.

References

[1]Rogers, J. W., Jr., and Agnes, G. S., "Modeling a Piezoelectric Beam String," *Journal of Spacecraft and Rockets*, Vol. 39, No. 5, 2002, pp. 725–731.

[2]Rogers, J., and Agnes, G., "Modeling a Piezoelectric Laminated Plate-Membrane," *Journal of Intelligent Material Systems and Structures*, Vol. 6, No. 10, 2002.

[3]Rogers, J. W., Jr., and Agnes, G. S., "Modeling Discontinuous Axisymmetric Active Optical Membranes," *Journal of Spacecraft and Rockets*, Vol. 40, No. 4, 2003, pp. 553–564.

[4]Nayfeh, A., *Problems in Perturbation*, Wiley, New York, 1993, pp. 318–323.

[5]Nayfeh, A., *Introduction to Perturbation Techniques*, Wiley, New York, 1981.

[6]Cook, R., Malkus, D., and Plesha, M., *Concepts and Applications of Finite Element Analysis*, 3rd ed., Wiley, New York, 1974, pp. 75–78.

[7]Meirovitch, L., *Elements of Vibration Analysis*, McGraw–Hill, New York, 1986, pp. 209–220.

Sunil Saigal
Associate Editor